



## A Robot Arm for Assisting Liver Surgery

Xie Xiaohui<sup>1</sup>, Na Qj<sup>2</sup>, Zhao Cuicui<sup>3</sup> and Du Ruxu<sup>4</sup>

<sup>1</sup>Shenzhen Institute of Advanced Technology, Chinese Academy of Sciences, xh.xie@siat.ac.cn

<sup>2</sup>Shenzhen Institute of Advanced Technology, Chinese Academy of Sciences, qi.na@siat.ac.cn

<sup>3</sup>Shenzhen Institute of Advanced Technology, Chinese Academy of Sciences, cc.zhao@siat.ac.cn

<sup>4</sup>Institute of Precision Engineering, The Chinese University of Hong Kong, rdu@acaе.cuhk.edu.hk

### ABSTRACT

Liver surgery is a complex operation. During the operation, even with the help of real-time CT imaging, doctors often struggle in finding the exact tumor positions. This paper introduces a robot arm specially designed for assisting liver surgery. It includes a 5 DOF (Degree-of-Freedom) robot arm and a computer software system. The position resolution of the robot arm is 0.1mm and the software system is developed using Visual C++. The robot arm can hold an endoscope. With the help of electromagnetic position tracking device, the robot arm can also show the path of the endoscope during the surgery. To test the accuracy of the robot arm, a prototype is designed and built. The experiment results show that the position accuracy of the robot arm is 0.3mm, sufficient for assisting liver surgery. In addition, the cost of this system is only about US\$10,000, much lower than the surgical robot systems in the market.

**Keywords:** robot, liver surgery, robot path generation.

**DOI:** 10.3722/cadaps.2011.713-722

### INTRODUCTION

With the rapid development of biomedical technology, Minimally Invasive Surgery (MIS) has become the trend for surgery today. MIS has many advantages such as preserving more healthy tissues, reducing wounds, and promoting rapid recovery. In order to make MIS more effective, various auxiliary systems are needed, such as real time CT imaging system and robot arm. In particular, the robot arm can help doctors to hold the endoscope steadily. It helps to reduce the difficulty of the surgery and shorten the time of surgery, and more importantly, the uncertainty of the manual operation. As a result, much research has been carried out [1][2][2]. In recent years, the technology has been gradually maturing, considering the safety [2], remote operation [5][6][7], learning control [8], vision guided control [9] and training [8].

This paper focuses on the robot. There have been a number of robots in the market. The medical robots, such as ZEUS and Da Vinci have powerful functions and can be used for many kinds of surgeries. However, they are also very expensive and hence, cannot be adopted by developing countries. The industry robots, such as KUKA and ABB, on the other hand, do not have the right size and configuration for surgery. According to literature survey, there have been a large number of papers on designing and controlling surgical robots [11][12][13][14][15][16][17][18][19].

In cooperation with the 1<sup>st</sup>Shenzhen Hospital, we designed and built a robot arm especially for liver surgery. This low cost robot can help doctors to hold the endoscope steadily, move in through a designed path, and visualize the endoscope position inside the patient during the operation.

This paper presents our robot. The rest of the paper is organized as follows: Section 2 introduces the configuration of the robot. Section 3 presents the motion control of the robot. Section 4 contains experiment results. Finally, Section 5 contains conclusions and future work.

## THE CONFIGURATION

According to surgery doctors, the key functions of the auxiliary robot shall include: (a) hold the endoscope steadily; (b) move the endoscope through a designed path avoiding important organs; and (c) visualize the motion of the endoscope throughout the operation.

To realize these functions, our robot has three Degree-of-Freedom(DOF)for positioning, as shown in Figure 1, and 2 DOF for orientation, as shown in Figure 2. Thus, it has a total of 5 DOF. We chose the Cartesian coordinate system for setting up the mechanism of the robot.

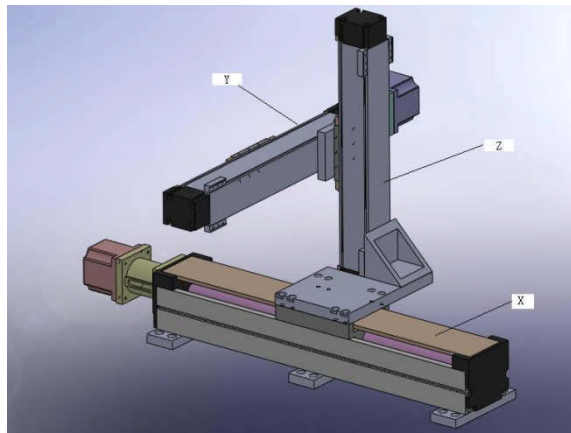


Fig. 1: The CAD model of the robot mainframe made of 3 translation axes.

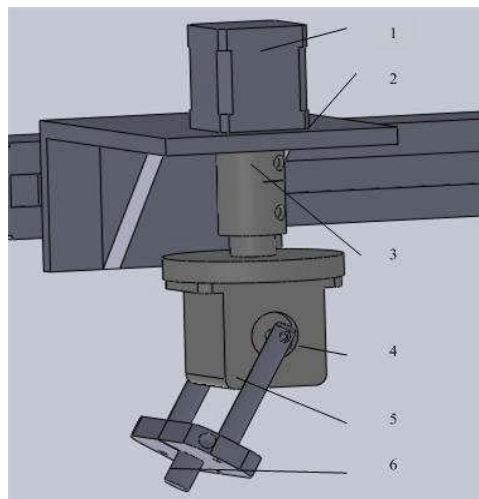


Fig. 2: The CAD model of the robot wrist: 1 - Z axis motor; 2 - support frame board; 3 - coupling connector; 4 - the pitch motor; 5 - swing arm motor; 6 actuator.

The three translation axes carry different amount of loading. The X axis is the largest. Its maximum loading is  $F_x = 1000\text{N}$ ,  $F_y = 400\text{N}$ , and  $F_z = 200\text{N}$  and its maximum torque is  $M_x = 10\text{Nm}$ ,  $M_y = 25\text{Nm}$ , and  $M_z = 25\text{Nm}$ . The Y and Z axes are the same. Their maximum loading is  $F_x = 350\text{N}$ ,  $F_y = 300\text{N}$ ,  $F_z = 400\text{N}$  and their maximum torque is  $M_x = 5\text{Nm}$ ,  $M_y = 15\text{Nm}$ ,  $M_z = 20\text{Nm}$ . The position accuracy of the three axes is the same and is  $0.023\text{mm}/300\text{mm}$ , and the repeatability is  $0.02\text{mm}/300\text{mm}$ .

The orientation wrist consists of two rotating joints. One rotates around Z axis and its rotation range is  $0^\circ \sim 360^\circ$ . It is driven by a step-motor mounted on the rotation plant and the motor is connected to a rotation plant by a coupling device. The other rotates about the rotation plant and its rotation range is  $0 \sim 75^\circ$ . It is also driven by a step-motor. Note that it is the pitch arm and thus, the pitch arm can rotate in Z-X plant. As shown in Figure 2, the axes of the two rotating joints intersect.



Fig. 3: The photo of the robot.

Figure 3 shows the photo of the robot. Its dimension is approximately  $362.78 \times 362.78 \times 248.20$  mm. The assembly of the robot is rather simple. In particular, as shown in Figure 4, each of the two rotation joints has two holes; one hole is on the fixed part and the other is on the rotation part. The assembly of the joints is done by plugging the locating pin into the locating hole.

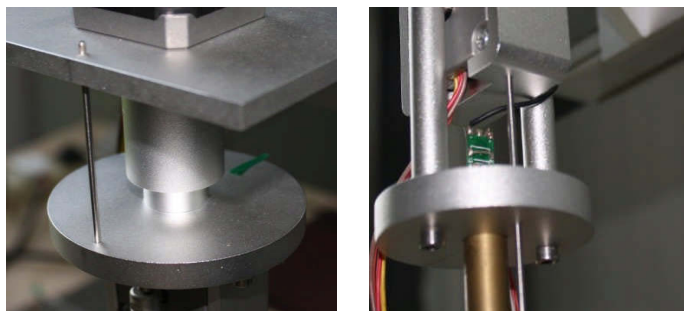


Fig. 4: (a) The photo of the rotary joint, (b) The photo of the pitch joint.

The end effector of the robot is a mounting plate that can hold an endoscope and a laser transmitter. The laser transmitter indicates the moving path of the endoscope. For protecting and calibrating the robot, nine photoelectric limit switches are adopted. They are mounted on the three translation axes. Each axis has three limit switches: two are used for limit protection the other is used as zero position calibration.

## THE MOTION CONTROL

Before surgery, the doctor would determine the surgical path of the endoscope in the virtual space of a computer. During the surgery, the robot would follow designed path and indicate the actual path. As illustrated in Figure 5, assuming Point C is the liver tumor and MC is the designed punctuation path. The robot will first adjust its posture, making the laser indicator line up to the surgical path MC. Then, it will moves along the line MC, carrying out the surgical operation.

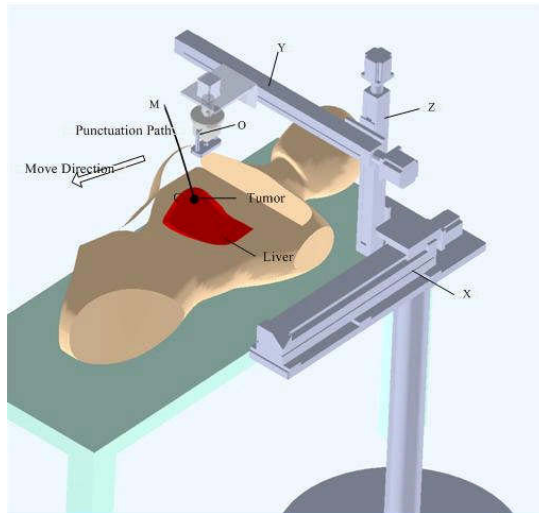


Fig. 5: Illustration of the robot operation during the surgery.

As shown in the previous section, the robot has five joints. The first three joints are translation joints, and the other two are rotation joints. We use the D-H method to analyze the movement of the robot. Figure 6 shows the coordinate system.

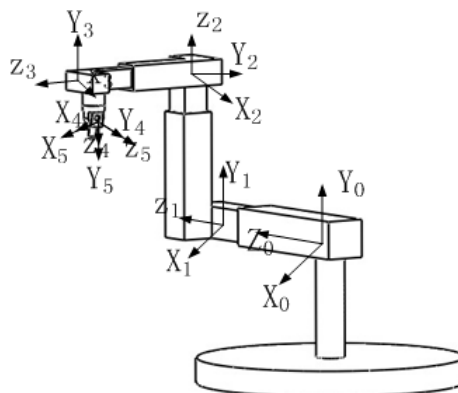


Fig. 6: Referenced coordinate system of mechanical arm joint.

Table 1 shows the key parameters of the robot, where  $a_i$  is the distance between  $Z_i$  and  $Z_{i+1}$  along  $X_i$  axis;  $\alpha_i$  is the angle  $Z_i$  and  $Z_{i+1}$  about the  $X_{i+1}$  axes;  $d_i$  is the distance from  $O_i$  to the intersection of  $X_{i+1}$  and  $Z_i$ ; and  $\theta_i$  is the angle between  $X_i$  and  $X_{i+1}$  about the  $Z_i$  axis.

Joint	$\theta$	$d$	$a$	$\alpha$
1	$0^\circ$	$l_1$	0	$0^\circ$
2	$90^\circ$	$l_2$	$a_2$	$-90^\circ$
3	$0^\circ$	$l_3$	$a_3$	$90^\circ$
4	$\theta_4$	$d_4$	$a_4$	$90^\circ$
5	$\theta_5$	0	0	$90^\circ$

Tab. 1: D-H parameters of the our robot

In table 1,  $l_1$ ,  $l_2$ , and  $l_3$  are the translations of the three linear axes,  $\theta_4$  and  $\theta_5$  are the rotations of the two rotating axes;  $a_2 = 103$  mm,  $a_3 = 82$  mm,  $a_4 = 110$  mm,  $d_4 = 91.5$  mm are all constants. Thus, the transform matrixes are:

$${}^1_0T = \begin{bmatrix} 1 & 0 & 0 & 0 \\ 0 & 1 & 0 & 0 \\ 0 & 0 & 1 & l_1 \\ 0 & 0 & 0 & 1 \end{bmatrix} \quad (1)$$

$${}^2_1T = \begin{bmatrix} 0 & -1 & 0 & a_2 \\ 0 & 0 & 1 & l_2 \\ -1 & 0 & 0 & 0 \\ 0 & 0 & 0 & 1 \end{bmatrix} \quad (2)$$

$${}^3_2T = \begin{bmatrix} 1 & 0 & 0 & a_3 \\ 0 & 0 & -1 & -l_3 \\ 0 & 1 & 0 & 0 \\ 0 & 0 & 0 & 1 \end{bmatrix} \quad (3)$$

$${}^4_3T = \begin{bmatrix} c\theta_4 & -s\theta_4 & 0 & a_4 \\ 0 & 0 & -1 & -d_4 \\ s\theta_4 & c\theta_4 & 0 & 0 \\ 0 & 0 & 0 & 1 \end{bmatrix} \quad (4)$$

$${}^5_4T = \begin{bmatrix} c\theta_5 & s\theta_5 & 0 & 0 \\ 0 & 0 & -1 & 0 \\ s\theta_5 & c\theta_5 & 0 & 0 \\ 0 & 0 & 0 & 1 \end{bmatrix} \quad (5)$$

Therefore, the global transform matrix is as follows:

$${}^q_0T = {}^0_1T {}^1_2T {}^2_3T {}^3_4T {}^4_5T \quad (6)$$

Or

$${}^5_0T = \begin{bmatrix} s\theta_4 c\theta_5 & -c\theta_4 s\theta_5 & -c\theta_4 & l_3 + a_2 \\ -s\theta_5 & -c\theta_5 & 0 & l_2 - d_4 \\ -c\theta_4 c\theta_5 & -c\theta_4 s\theta_5 & -s\theta_4 & l_1 - a_3 - a_4 \\ 0 & 0 & 0 & 1 \end{bmatrix} \quad (7)$$

Plug in the parameters in Table 1 into Equation (7), the transformation matrix is:

$$T = \begin{bmatrix} 1 & 0 & 0 & 103 \\ 0 & 1 & 0 & -91.5 \\ 0 & 0 & 1 & -192 \\ 0 & 0 & 0 & 1 \end{bmatrix}$$

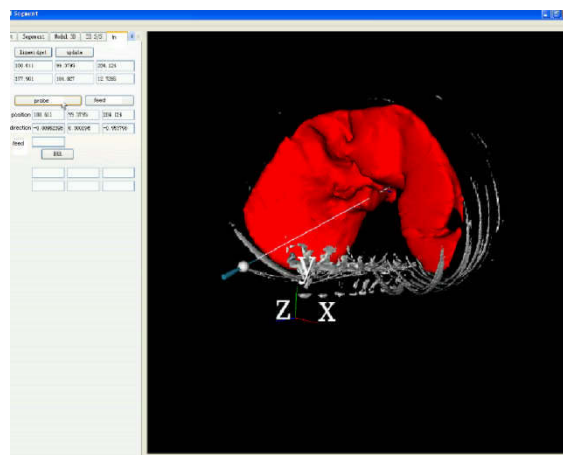


Fig. 7: Planning of punctuation path.

Figure 7 shows the computer interface for the surgical path planning. Before the surgery, the liver CT of the patient was got and the three-dimensional image can be reconstructed. Then the doctor can determine the punctuation path in the surgery.

## EXPERIMENT RESULTS

Figure 8 shows the robot prototype with the computer display. In particularly, an electromagnetic position tracking device is used to test the accuracy of the motion. The receiver of the electromagnetic position tracking device is fixed on a set position while the emitter is fixed on the end effector of the robot. When the emitter moves with the end effector, the receiver will indicate the motion trajectory point-by-point. The accuracy can then be assessed by comparing the designed trajectory and the actual motion trajectory.



Fig. 8: The robot prototype and the experiment setup: (a) the system setup, (b) the three translation axes, (c) the rotating platform, (d) the pitch axis.

In the experiment, the X and Y axes are set to move 300 mm, and the Z axis is set to move 200 mm. The speed is set 5mm/s for all axes. For the orientation, the rotation angle of the rotation joint is set to change from 0 to 180°, and the pitch joint is set to change from 0 to 45°. The speed is 5°/s. In each case, 15 tests are carried out. The experiment results are shown in Figures9 and 10.

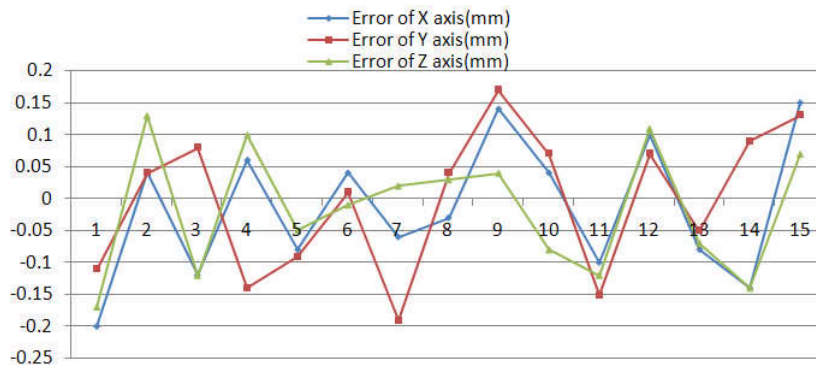


Fig. 9: The error of the translation axes (mm).

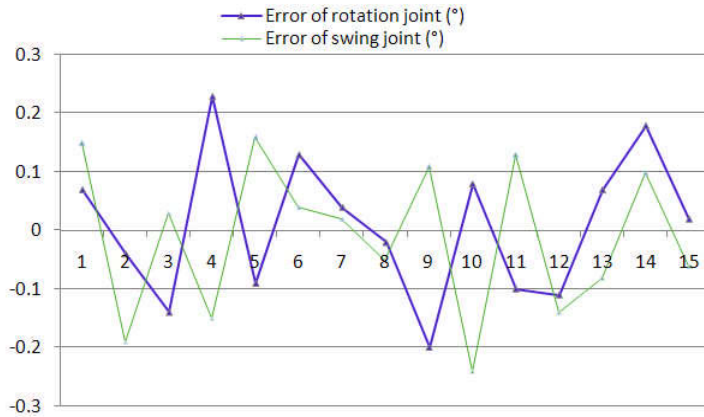


Fig. 10: The error of the orientation axes (°).

To evaluate the location accuracy, we use the maximum error and the sum-of-square error defined below:

$$\sigma = \sqrt{\frac{\sum (x_i - \mu)^2}{n}} \quad (8)$$

Where,  $\mu = \frac{1}{n} \sum x_i$ .

Based on the data above, it is found that the maximum error are  $|X_{MAX}| = 0.20\text{mm}$ ,  $|Y_{MAX}| = 0.19\text{mm}$ ,  $|Z_{MAX}| = 0.17\text{mm}$ ,  $\sigma_x = 0.148\text{mm}$ ,  $\sigma_y = 0.118\text{mm}$ , and  $\sigma_z = 0.178\text{mm}$ . Therefore, the total maximum error and the total sum-of-squares error are:

$$d_{MAX} = \sqrt{x_{MAX}^2 + y_{MAX}^2 + z_{MAX}^2} = 0.324 \text{ mm}$$

$$\sigma = \sqrt{\sigma_x^2 + \sigma_y^2 + \sigma_z^2} = 0.260\text{mm}$$

Moreover, the maximum error and the sum-of-squares error of the rotating axis and the pitch axis are  $|\alpha_{MAX}| = 0.23^\circ$ ,  $|\beta_{MAX}| = 0.24^\circ$ ,  $\sigma_\alpha = 0.1892^\circ$ , and  $\sigma_\beta = 0.3035^\circ$ .

The second set of experiments involves the five axes moving altogether. Figure 11 shows the experiment results. Figure 11(a) the positions of the effector: the large red mark is the designed position while the other marks are the 15 experiment results. Figure 11(b) shows the maximum errors of the 15 experiments. The average of the maximum error is 0.3 mm and the maximum of the maximum error is 0.45 mm.

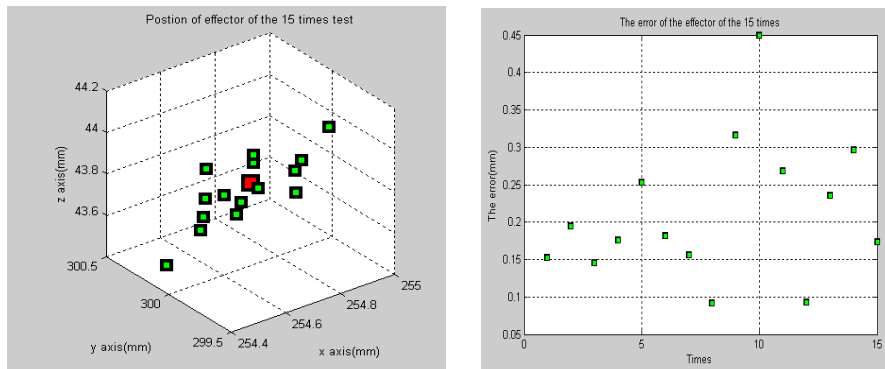


Fig. 11: (a) The positions of the actuator from the experiment, (b) The deviation of the actuator in the experiment.

## CONCLUSIONS AND FUTURE WORK

This paper introduces a low-cost robot arm for assisting liver surgery. The robot arm consists of 3 linear axes and 2 rotary axes. Its end effector includes a holder for endoscope and a laser prob. The experiment results show that the accuracy of the robot is 0.3 mm, sufficient for assisting liver surgery.

In the near future, animal tests would be carried out.

## ACKNOWLEDGMENT

This paper is partially supported by the National Natural Science Foundation of China (No. 60805047) and the State Key Laboratory of Robotics and System (HIT) (No. SKLRS200704).

## REFERENCES

- [1] Ruurda, J. P.; Vroohhoven, R. V.; Broeders, I.: A New Era in Laparoscopic Surgery, Robot-Assisted Surgical Systems, *Ann R Coll Surg Engl.*, 84(4), 2002, 223–226. (DOI:10.1308/003588402320439621)
- [2] Dario, P.; Guglielmelli, E.; Allotta, B.; Carrozza, M. C.: Robotics for Medical Applications, *IEEE Robotics and Automation Magazine*, 9, 1996, 44-56. (DOI:10.1109/100.540149)
- [3] Sackier, J. M.; Wang, Y.: Robotically Assisted Laparoscopic Surgery: from Concept to Development, *Surgical Endoscopy*, 8, 1994, 63-66. (DOI:10.1007/BF02909496)
- [4] Fei, B. W.; Wan, S. N.: The Safety Issues of Medical Robotics, *Reliability Engineering and System Safety*, 73, 2001, 183-192. (DOI:10.1016/S0951-8320(01)00037-0)
- [5] Mitsuishi, M.; Hzuka, Y.; Watanabe, H.; Hashizume, H.: Remote Operation of a Microsurgical System, *IEEE International Conference on Robotics & Automation*, 1998, 1013-1019. (DOI:10.1109/ROBOT.1998.677220)
- [6] Ghodoussi, M.; Butner, S. E.; Wang, Y.: Robotic Surgery— the Transatlantic Case, *Proc., IEEE Int. Conf. on Robotics & Automation*, 5, 2002, 1882-1888. (DOI:10.1109/ROBOT.2002.1014815)
- [7] Markscaux, J.; Leroy, J.; Gangnerm et al: Transatlantic Robot—Assisted Telesurgery: ATM Technology Now Enables Operations to be Performed over Huge Distances, *Nature*, 27(9), 2001, 379-380. (DOI:10.1038/35096636)
- [8] Jacobs, L. K.; Shayani, V.; Sackier, J. M.: Determination of the Learning Curve of the AESOP Robot, *SurgEndosc*, 11, 1997, 54-55. (DOI: 10.1007/s004649900294)
- [9] Wang, Y. F.; Uecker, D. R.; Lun, W. Y.: Choreographed Scope Maneuvering in Robotically-Assisted Laparoscopy with Active Vision Guidance, *Proceedings 3rd IEEE Workshop on Applications of Computer Vision*, 1996, 187~192. (DOI:10.1109/ACV.1996.572054)

- [10] Dankelman, J.: Surgical Robots and Other Training Tools in Minimally Invasive Surgery, IEEE International Conference on Systems, Man and Cybernetics, 2004, 2459-2464.(DOI: 10.1109/ICSMC.2004.1400699)
- [11] Butner, S. E.; Ghodoussi, M.: Transforming a Suring Robot for Human Telesurgery, IEEE Transactions on Robotics and Automation, 19, 2003, 818-824.(DOI:10.1109/TRA.2003.817214)
- [12] Noonan, D. P.; Mylonas, G. P.; Darzi, A.; Yang, G. Z.: Gaze Contingent Articulated Robot Control for Robot Assisted Minimally Invasive Surgery, IEEE/RSJ Int. Conf. on Intelligent Robotics and Systems, 2008, 1186-1191.(DOI:10.1109/IROS.2008.4651105)
- [13] Gulat, S.; Jung, E. H.; Kapoor, C.: Execution Engine for Robotic Surgery Support Functions in an Unmanned Operating Room, IEEE Int. Conf. on Robotics and Automation, 2007, 404-409.(DOI: 10.1109/CIRA.2007.382913)
- [14] Burdea, C. G.; Dunnm, S. M.; Levy, G.: Evaluation of Robot Based Registration for Subtraction Radiography, Medical Image Analysis, 3, 1999, 265-274.(DOI:10.1016/S1361-8415(99)80023-1)
- [15] Funda, J.; Taylor, R. H. et al: Constrained Cartesian Motion Controller Teleoperated Surgical Robots, IEEE Transaction on Robotics and Automation, 12(3), 1996, 453-465.(DOI:10.1109/70.499826)
- [16] Taylor, R.; Jensen, P. et al: A Steady-hand Robotic System for Micro Surgical Augmentation, Int. J. of Robotics Research, 18, 1999, 1201-1210.(DOI: 10.1177/02783649922067807)
- [17] Boctor, E. M.; Webster, J. R. et al: Robotically Assisted Ablative Treatment Guided by Freehand 3D Ultrasound, Computer Assisted Radiology and Surgery, 1268, 2004, 503-508.(DOI:10.1016/j.ics.2004.03.261)
- [18] Hummel, J.; Jun, C. M.; Bax, M.; and et al.: Standardized Evaluation Method for Electromagnetic Tracking Systems, Medical Image 2005: Visualization, Image-Guided Procedures and Display, 2005, 236-240.(DOI:10.1117/12.595256)
- [19] Hong, J.; Nakashima, H.; Konishi, K. et al: Interventional Navigation for Abdominal Therapy Based on Simultaneous Use of MRI and Ultrasound, Medical and Biological Engineering and Computing, 2006, 44, 1127-1134.(DOI:10.1007/s11517-006-0133-2)